Biology Direct

RESEARCH

Open Access

Multiplex antimicrobial activities of the self-assembled amphiphilic polypeptide β nanofiber KF-5 against vaginal pathogens

Ling Fang[1,2,3†], Tiancheng Yang[1,3†], Haojue Wang[2*] and Jun Cao[1,3*]

Abstract

Background Vaginal infections caused by multidrug-resistant pathogens such as *Candida albicans* and *Gardnerella* spp. represent a significant health challenge. Current treatments often fail because of resistance and toxicity. This study aimed to synthesize and characterize a novel amphiphilic polypeptide, KF-5, and evaluate its antibacterial and antifungal activities, biocompatibility, and potential mechanisms of action.

Results The KF-5 peptide was synthesized via solid-phase peptide synthesis and self-assembled into nanostructures with filamentous and hydrogel-like configurations. Characterization by scanning electron microscopy (SEM), transmission electron microscopy (TEM), and atomic force microscopy (AFM) confirmed the unique nanostructural properties of KF-5. KF-5 (125, 250, or 500 μg/ml) demonstrated potent antibacterial and antifungal activities, with significant inhibitory effects on drug-resistant *Candida albicans* and *Gardnerella* spp. ($P < 0.05$). In vitro assays revealed that 500 μg/ml KF-5 disrupted microbial cell membranes, increased membrane permeability, and induced lipid oxidation, leading to cell death ($P < 0.05$). Cytotoxicity tests revealed minimal toxicity in human vaginal epithelial cells, keratinocytes, and macrophages, with over 95% viability at high concentrations. Molecular dynamics simulations indicated that KF-5 interacts with phospholipid bilayers through electrostatic interactions, causing membrane disruption. In vivo studies using a mouse model of vaginal infection revealed that 0.5, 1, and 2 mg/ml KF-5 significantly reduced fungal burden and inflammation, and histological analysis confirmed the restoration of vaginal mucosal integrity ($P < 0.01$). Compared with conventional antifungal treatments such as miconazole, KF-5 exhibited superior efficacy ($P < 0.01$).

Conclusions KF-5 demonstrates significant potential as a safe and effective antimicrobial agent for treating vaginal infections. Its ability to disrupt microbial membranes while maintaining biocompatibility with human cells highlights its potential for clinical application. These findings provide a foundation for further development of KF-5 as a therapeutic option for combating drug-resistant infections.

Keywords Self-assembled peptide nanoscale, Antibacterial, Bacterial biofilm, Vaginal infections

†Ling Fang and Tiancheng Yang have made equal contributions to this work.

*Correspondence:
Haojue Wang
xishanwanghao@163.com
Jun Cao
caojuncn@hotmail.com
Full list of author information is available at the end of the article

Introduction

Vaginal infections are common gynecological conditions that significantly affect the health and quality of life of women of all ages [1]. The vaginal microbiome is uniquely complex and differs considerably from that of other body sites, potentially influencing various health conditions [2]. Disruption of the vaginal microecosystem often leads to vaginal infection, inflammation, or imbalance in normal bacteria [1, 3]. Bacterial vaginosis, vulvovaginal candidiasis, and trichomoniasis are the most common types of vaginal infection. Bacterial vaginosis, with an incidence rate of 9–50%, affects 23–29% of women globally, resulting in an annual treatment cost of $4.8 billion [4, 5]. Standard treatment options include oral metronidazole, intravaginal metronidazole, or clindamycin [1, 6], whereas vulvovaginal candidiasis typically requires oral fluconazole or topical azole drugs [7]. However, antibiotic therapy often leads to drug resistance and interactions between various pathogenic bacteria can result in robust biofilm formation, contributing to disease recurrence [8, 9]. Studies have confirmed that multilayered bacterial biofilm matrices play a crucial role in counteracting the antimicrobial effects of various chemical agents. These bacteria develop resistance to multiple antibiotics, which is sometimes more than 1000 times greater than that of planktonic cells [10–12]. Biofilms are considered the cause of 80% of chronic microbial infections [13, 14]. Given the lack of specific drugs in clinical practice, development of novel antimicrobial agents may significantly improve the treatment of vaginal infections.

Antimicrobial peptides (AMPs), crucial components of the mammalian defense system, are characterized by high thermal stability, good water solubility, broad-spectrum sterilization capacity, and the ability to eliminate fungi and protozoa [15, 16]. In recent decades, AMPs have rapidly evolved and have gained attention as potential therapeutic agents. Bioextracted AMPs demonstrate good biocompatibility, whereas chemically synthesized AMPs are easily mass-produced, making them suitable for gene engineering [16–18]. Nanomaterials are composed of individual units 1–100 nm in size. Owing to their exceptional physicochemical properties arising from their high surface area and nanoscale size, nanomaterials have great potential in pharmaceutical and biomedical fields, cancer treatment, drug/gene delivery, medical implantation, and biological imaging [19]. Peptide-based nanostructures can be endowed with specific functionalities by exploiting the reactivity of amino acid side chains for covalent linking of bioactive groups or conjugation with biocompatible polymers, nucleic acid segments, fatty acids, or glycans [20]. Owing to their high biocompatibility, chemical diversity, and high load capacity, self-assembled peptide nanomaterials have found extensive application in regenerative medicine and drug delivery [21–23]. However, the inherent antibacterial activity of peptide-based nanostructures has been underexplored, with previous peptide assembly based studies predominantly focusing on the comparatively long peptides and polypeptides that form hydrogels. AMPs can self-assemble into various nanostructures, such as α-defensin 6, as well as peptides secreted by bacteria that stabilize through noncovalent interactions, such as hydrogen bonding, hydrophobic interactions, and π-π stacking, forming fibrous amyloid-like nanostructures that function in innate immunity [24–27]. Notably, self-assembled AMP nanostructures retain their self-assembly and AMP properties [28, 29].

In recent years, numerous studies have demonstrated the antimicrobial activities of amyloid proteins and peptides. These AMPs are secreted by cells and exhibit potent neurotoxic effects after precipitation and accumulation within the cell matrix [30, 31]. Research suggests that amyloid proteins form transmembrane pores in lipid membranes, a mechanism akin to how AMPs disrupt bacterial membranes to induce osmosis [32, 33]. Amyloid-β peptide (Aβ), which is found in β-amyloid plaques, plays a critical role in Alzheimer's disease (AD) [34, 35]. Moreover, Aβ has been identified as an AMP and its deposition is considered a protective innate immune response to infection [33, 36, 37]. Both Aβ 1–40 and Aβ 1–42 display antibacterial, antiyeast, and antiviral activities, which supports the notion that Aβ peptides are potential natural antimicrobial agents, elucidates the antiviral mechanism of Aβ peptides, and suggests a possible connection between HSV-1 infection and latency, Aβ peptides, and the sporadic form of AD [36].

In this study, we aimed to extract core fragments from human amyloid proteins and chemically synthesize the amphiphilic peptide, KF-5. This KF-5 polypeptide can self-assemble into a β-nanofiber structure in aqueous solutions. We further explored the effects of KF-5 polypeptide on common vaginal infection pathogens and the underlying mechanisms. The results demonstrated that these amyloid peptides could self-assemble into nanostructures that exhibited bactericidal effects. This study provides a novel strategy for designing AMPs from the self-assembly and antibacterial perspectives, potentially offering a new approach for treating vaginal infections.

Materials and methods

Materials

All the peptides (purity > 95%) were purchased from GL Biochem (Shanghai, China). Glutaraldehyde (2.5%) was acquired from Sigma-Aldrich Co. Ltd. (St. Louis, MO, USA). Salt compounds were obtained from Shanghai Macklin Biochemical Co. Ltd. (Shanghai, China). Propidium iodide (PI) and 8-anilinonapthalene-1-sulfonic acid

(ANS) were obtained from Beyotime (Shanghai, China) and Shanghai Bepharm Science and Technology Co. Ltd. (Shanghai, China). SYTO9 green fluorescent nucleic acid stain was obtained from Thermo Fisher (Waltham, MA, USA), and 3,3′-dipropylthiadicarbocyanine iodide (diSC3(5)) was purchased from Shanghai Bepharm Science & Technology Co., Ltd. (Shanghai, China). Tryptone, brain heart infusion (BHI), porcine skin (LP0008), yeast extract (LP0021), glucose, starch, and drug-sensitive pieces were obtained from Oxoid (Basingstoke, UK). Columbia blood agar plates were obtained from CrMicro (Jiangmen, Guangdong, China). Dimethyl sulfoxide (DMSO) and agar were obtained from Sangon Biotech (Shanghai, China). *Gardnerella* spp. and *Candida albicans* (American Type Culture Collection (ATCC), Manassas, VA, USA, 10231) were obtained from ATCC (cat. no. 14018, Manassas, VA, USA) and the Institute of Microbiology of the Chinese Academy of Science, respectively.

Preparation of samples

The peptide powder was dissolved in ultrapure water to a final concentration of 5 mg/mL. The solution was ultrasonicated for 10 min at room temperature and a frequency of 40 kHz. After ultrasonication, the samples were gradually cooled to 25 °C and left overnight for stabilization. The prepared samples were stable when stored at room temperature for up to 90 d without significant degradation [38].

Microbial culture

Gardnerella spp. were obtained from the ATCC, Manassas, VA, USA (Cat. No. 14018). Vaginal clinical isolates were collected via vaginal swabs from Xishan People's Hospital (based on the Nugent score: BV ≥ 7 points). After immediate inoculation on Columbia blood agar plates, bacteria were maintained in an anaerobic environment with 5% CO_2 at 37 °C for 48 h. Matrix-assisted laser desorption/ionization time-of-flight (MALDI-TOF, Bruker Daltonics, Billerica, MA, USA) was used to identify the candidate *Gardnerella spp*. *Gardnerella* spp. were maintained in BHI broth (Oxoid, Basingstoke, UK) supplemented with BHI broth supplemented with 1% yeast extract (Oxoid, Basingstoke, UK), 1% gelatin (Oxoid, Basingstoke, UK), 0.1% glucose (Oxoid, Basingstoke, UK), 0.1% soluble starch (Oxoid, Basingstoke, UK), and 10% fetal bovine serum (FBS) (Oxoid, Basingstoke, UK).

Candida albicans spores were cultured in Sabouraud medium. Sabouraud medium consisted of 20 g agar (Crmicro, Jiangmen, Guangdong, China) and 40 g glucose (Oxoid, Basingstoke, UK) supplemented with distilled water to a volume of 1 L, which was subsequently sterilized at 115 °C for 20 min using high-pressure steam. The solid Sabouraud medium consisted of 10 g peptone (Oxoid, Basingstoke, UK), 20 g agar (Oxoid, Basingstoke, UK), and 40 g glucose (Oxoid, Basingstoke, UK) and was supplemented with 1 L distilled water, after which the mixture was heated at 115 °C for 20 min with high-pressure steam for sterilization. *Candida albicans* mycelia were induced by adding 10% FBS (Oxoid, Basingstoke, UK) to the Sabouraud medium.

Reversed-phase high-performance liquid chromatography (HPLC) and mass spectrometry (MS) analysis

Reverse-phase HPLC (LC Agilent, Agilent Technologies, Boblingen, Germany) of the gel formulation was performed using a reversed-phase Ultra Aqueous C18 analytical column (2.1 mm × 100 mm, 5 μm, Agilent, Boblingen, Germany). Elution was performed using a 30–60% gradient of acetonitrile in water and 0.05% trifluoroacetic acid (TFA). The column eluate was monitored using a photodiode-array detector. After purification, the peptides were characterized by electrospray ionization MS (ESI–MS) using a QStar Elite hybrid LC–MS/MS system.

Rheological analysis

The resulting disk-shaped composite hydrogels were placed on the stage of a rheometer (MCR-502, Anton Paar, Graz, Austria) with a parallel plate geometry. The linear dynamic viscoelasticity was determined in the shear mode at a 1% strain amplitude for frequency sweeps.

Observation of the nanostructures of the peptide samples

Transmission electron microscopy (TEM) images were captured using a JEM1200EX instrument (JEOL Ltd., Tokyo, Japan) operating at 100 kV and dropped onto a double copper net. The samples (1 mg/ml were diluted tenfold and stained with 3% uranyl acetate for observation.

For atomic force microscopy (AFM), 1 mL of liquid KF-5 was dropped onto a mica sheet and observed using a Bruker Dension Icon (Karlsruhe, Germany).

For scanning electron microscopy (SEM), polypeptide samples were freeze-dried, pasted onto a platform with conductive adhesive, compacted, and the unfixed sample was blown away. The samples were subsequently sprayed with gold, and a scanning electron microscope (Zeiss Supra 55, Oberkochen, Germany) was used for observation.

Fourier transform infrared (FTIR) spectroscopy was performed on the film of each sample using a MATTSON 3000 FT-IR spectrophotometer (Madison, WI, USA) with a wavenumber range of 400–4000 cm^{-1} and resolution of 4 cm^{-1}.

Characterization via spectroscopy and zeta potential determination

A Chirascan Plus instrument (Applied Photophysics Ltd., Leatherhead, UK) was used to analyze conformational changes in the peptide samples at 190–260 nm. The spectra were recorded at an absorbance of $A < 2$ at any measured point, with the time per point, step size, and bandwidth set at 0.5 s, 1 nm, and 1 nm, respectively. The temperature was maintained at 25 °C. Circular dichroism (CD) data were collected at 20, 30, 40, 50, 60, 70, 80, 90, and 95 °C to evaluate the secondary structures of the samples. For zeta potential measurements, the samples were diluted to various pH values (3, 5, 7, 9, and 11) in hydrogen chloride (HCL) and sodium hydroxide (NaOH) solutions (Oxoid, Basingstoke, UK). A particle size and potential analyzer (NANO ZS90, Malvern Instruments Ltd., Malvern, UK) was used to determine zeta potential and particle size.

Evaluation of the activity of KF-5 against bacteria and fungi

Candida albicans (cat. no. 10231; ATCC, Manassas, VA, USA) was used for all experiments. Multidrug-resistant strains (*Candida albicans* 3147, resistant to fluconazole, amphotericin B, and voriconazole; *Gardnerella* spp. AmMS 117, resistant to metronidazole, erythromycin, and gentamicin) were obtained from the Xishan People's Hospital of Wuxi City. Initially, *Candida albicans* stored at − 80 °C was thawed and inoculated into Sabouraud liquid medium with overnight shaking. *Candida albicans* was subsequently transferred to fresh medium and incubated for 6–8 h to culture the fungi. The amount of *Candida albicans* added reached 10^7 colony-forming units (CFU)/mL. *Candida albicans* (100 μL) was mixed with KF-5 solution (100 μL) at concentrations of 0, 125, 250, and 500 μg/mL in 800 μL of sterile water for 3 h. Then, 100 μL of the various dilutions of the mixed solution was evenly spread on Sabouraud's medium and maintained at 37 °C for 24–48 h before the CFUs were counted.

Permeability measurements were performed using the 8-anilinonapthalene-1-sulfonic acid (ANS) uptake assay. Next, 20 μM ANS (Beyotime, Shanghai, China) and 10^7 CFU/mL *Candida albicans* were mixed in 0.9% NaCl (Macklin Biochemical Co., Ltd., Shanghai, China) and incubated in the dark for 30 min. After centrifugation at 3000×*g* for 15 min using a Kubota centrifuge (Tokyo, Japan), samples were washed and resuspended in 0.9% NaCl (Macklin Biochemical Co., Ltd.). Next, 0 (blank control), 500 μg/mL KF-5, or melittin (positive control for permeabilization) were added to the suspension. Fluorescence emission changes were measured between 450 and 600 nm, with excitation at 380 nm, and recordings were taken for at least 60 min using a Costar Black microplate plate.

Depolarization measurements were performed using the diSC3 (5) uptake assay with processing steps similar to those described above (diSC3(5), 4 μM; excitation at 622 nm and emission at 670 nm; Bepharm Science & Technology Co., Ltd., Shanghai, China). Triton X-100 (a positive control for depolarization) was used as the control for membrane depolarization. Changes in fluorescence were measured and recordings were continued for at least 60 min.

Stability assay

KF-5 polypeptide nanohydrogels were stored in polypropylene bottles (Qorpak, Bridgeville, PA, USA) at different temperatures (4 °C, room temperature (25 °C), 30 °C, and 40 °C) for up to 8 weeks. The samples were removed weekly for analysis. Physical stability was evaluated by measuring pH using a microprobe electrode (Mettler Toledo, Greifensee, Switzerland), and viscosity was evaluated using a rotational viscometer (Shjingmi Co., Ltd., Shanghai, China). These measurements were performed on samples stored at 40 °C for eight weeks.

Antibacterial efficacy was assessed by determining the antibacterial effect of KF-5 using the method described in Section "Evaluation of the activity of KF-5 against bacteria and fungi". This test was performed on samples stored at all specified temperatures (4 °C, room temperature, 30 °C, and 40 °C) for up to eight weeks.

Lipid oxidation detection

Briefly, after treatment with KF-5, 10^7 CFU/mL *Candida albicans* (10 μL) was incubated with 10 μM C11-BODIPY581/591 (Glpbio, Montclair, CA, USA) for 60 min to detect lipid peroxidation. After washing twice with phosphate-buffered saline (PBS) (Oxoid, Basingstoke, UK), the labeled *Candida albicans* was trypsinized and resuspended in PBS supplemented with 5% FBS (Oxoid, Basingstoke, UK). The fluorescence emission changes induced by C11-BODIPY581/591 oxidation were examined at 525 nm with 488 nm excitation.

Confocal microscopy of Candida albicans and Gardnerella spp.

Confocal microscopy was used to observe the 3D structures of *Candida albicans* and *Gardnerella spp*. The biofilm surface was stained with 1 μg/mL PI and Syto9 staining solution (5×10^{-6} M) and incubated for 20 min in the dark. After washing twice with 0.9% NaCl, the samples were analyzed using an FV1000 laser confocal microscope (OLYMPUS, Tokyo, Japan).

Cell cytotoxicity experiments

The cytotoxicity of KF-5 to VK2 cells (vaginal keratinocytes; ATCC CRL-2616), HaCaT cells (human

keratinocytes), and RAW264.7 cells (murine macrophages) was measured using the Cell Counting Kit-8 (CCK-8; Beyotime, Shanghai, China). DMSO (Sangon Biotech, Shanghai, China) was used as the positive control. The CCK-8 method determines the number of live cells by detecting dehydrogenase activity in live cells, indirectly indicating cytotoxicity; that is, the measured absorbance is inversely proportional to the degree of cytotoxicity. VK2 cells were plated in sterile 96-well plates (5000 cells/well) and cultured in Dulbecco's modified Eagle's medium (DMEM) (Sigma–Aldrich Co., Ltd., St. Louis, MO, USA) supplemented with 10% FBS at 37 °C with 5% CO_2 for 12 h. Subsequently, VK2 cells were stimulated with gradient concentrations of KF-5 (125, 250, 500, and 1000 μg/mL) for 24 h. DMSO (1.25, 2.5, 5, or 10%) was used as a positive control. Each well was then supplemented with 10 μL of CCK-8 reagent and cultured for another 2 h. Cell viability was determined at 532 nm using a microplate reader (ELX 800MS; BioTek Instrument Inc., Winooski, VT, USA); with untreated cells serving as the negative control. Percentage viability was assessed by dividing the optical density (OD) of the treatment group by the OD of the respective vehicle control multiplied by 100. The cytotoxic effect of KF-5 was also evaluated in HaCaT and RAW264.7 cells following the same procedure described above.

Computational details

All simulations were performed using the GROMACS [39] (version 2021.2) simulation package, and Amber14SB [40] was used for the peptide KLVFF. The system consisted of 10 KLVFF peptides. The TIP3P water model was used to describe the water molecules, and 1-palmitoyl-2-oleoyl-sn-glycero-3-phosphocholine (POPC) was chosen as the cell membrane. There were 128 lipid molecules for each membrane model, and the CHARMM36 force field was used for POPC. Molecular dynamics simulations under an isothermal isobaric ensemble (NPT-Ensemble) after thousands of steps of energy minimization were implemented using the Berendsen method under 1 atm along the norm of the surface at 298 K for an equilibration period of 5 ns. Subsequent 50 ns production runs were carried out for each system via the nose–hoover and Parrinello–Rahman coupling methods. A cutoff scheme was implemented at 1.2 nm for the nonbonded interactions, and the particle mesh Ewald method [41] with a Fourier spacing of 0.1 nm was applied for the long-range electrostatic interactions. All covalent bonds were constrained using a linear constraint solver (LINCS) algorithm [42].

Animal experiments

All experimental procedures were approved by the Ethics Committee of Nanjing Medical University. BALB/c mice (female; 18–20 g; n = 6 per group) were purchased from GemPharmatech Co., Ltd. (Nanjing, Jiangsu, China) and had free access to water and food in an air-conditioned room at 23–25 °C and 50–60% humidity under a 12-h/12-h light/dark cycle. The mice were kept in the room for 7 days to allow them to adapt to the environment. The mice were randomly divided into five groups: the control group, model group, 0.5 mg/ml KF-5 group, 1 mg/ml KF-5 group, and 2 mg/ml KF-5 group. All mice, except those in the control group, were subcutaneously injected with 0.1 mL of β-estradiol (0.2 mg/mL, Sigma–Aldrich, St. Louis, MO, USA) once every two days for six days. For vaginal infection, 20 μl of *Candida albicans* solution (1×10^9 CFU/ml) was injected into the vagina once a day for a total of seven days after estradiol treatment. After modeling, the mice were intravaginally injected with different concentrations of KF-5 (0.5 mg/ml, 1 mg/ml, and 2 mg/ml) once daily for five days (20 μL/day). To evaluate the therapeutic effect of miconazole, the model mice were intravaginally injected with 0.5 mg/kg miconazole (MedChemExpress, Monmouth Junction, NJ, USA) once a day for five days (20 μL per day). Miconazole was suspended in 5% DMSO. The vagina was washed repeatedly with PBS and 100 μL of vaginal lavage fluid was collected for colony counting. Then, 10 μL of lavage fluid was subjected to Gram staining (Thermo Fisher Scientific, Waltham, MA, USA) to estimate hyphal formation. The mice were sacrificed and vaginal samples were collected and fixed with 4% paraformaldehyde (Thermo Fisher, Waltham, MA, USA), followed by hematoxylin and eosin (H&E; Sigma–Aldrich Co., Ltd., St. Louis, MO, USA) and periodic acid-Schiff (PAS) staining (Beyotime, Shanghai, China).

For the in vivo safety study, BALB/c mice (female; 18–20 g; n = 6 per group) were randomly divided into four groups: control (blank control), 0.5 mg/ml KF-5, 1 mg/ml KF-5, and 2 mg/ml KF-5. Mice were treated intravaginally with different concentrations of KF-5 or PBS (vehicle control) once a day for 28 days. Throughout the study, mice were monitored daily for signs of discomfort or toxicity. After 28 days, the mice were euthanized and vaginal samples were collected for analysis.

Enzyme-linked immunosorbent assay (ELISA)

First, the vaginal tissues were kept on ice and cut into approximately 1 mm^3 cubes via a razor blade on a glass plate before the lysate was acquired. The cubes were subsequently transferred to a handheld Potter S homogenizer (Sigma-Aldrich Co., Ltd., St. Louis, MO,

USA). The liquefied tissue was poured into 1.5 mL tubes and subjected to centrifugation at 10,000×*g* for 3 min at 4 °C. For cytokine analysis, supernatants from vaginal tissue homogenates were collected and transferred to 96-well ELISA plates. The concentrations of tumor necrosis factor-alpha (TNF-α) and interleukin-6 (IL-6) were determined using ELISA kits (R&D Systems, Minneapolis, MN, USA), in accordance with the manufacturer's instructions.

Statistical analysis

Each experiment was performed three times, and the results are presented as mean ± standard deviation (SDs). GraphPad Prism 8.0 was used for data analysis. For normally distributed data, a t-test was used for comparisons between two groups, and a one-way analysis of variance (ANOVA) followed by Tukey's post-hoc test was applied for multigroup comparisons. For non-normally distributed data, the Mann–Whitney U test or Kruskal–Wallis test was used as appropriate. Statistical significance was set at $P < 0.05$.

Results

Synthesis and physicochemical properties of KF-5

The KF-5 peptide was swiftly synthesized via solid-phase peptide synthesis technology, and HPLC analysis and MS confirmed its successful synthesis (Fig. 1A-B). HPLC analysis revealed a peak at a 6 min retention time of 9.35, and the calculated purity of the KF-5 peptide was 98.7029% based on the HPLC peak area integral (Table 1). MS analysis revealed that the mass of the target product was 651.4, which was consistent with the theoretical molecular weight of 652.8 (resulting from the removal of one H +) (Fig. 1B).

Table 1 KF-5 HPLC analysis

Rank	Time	Conc	Area	Height
1	4.975	0.4864	24,536	3909
2	8.482	0.6051	30,523	4814
3	9.356	98.7029	4,978,676	380,059
4	9.708	0.2056	10,371	5021
Total		100	5,044,106	393,803

Characterization of KF-5

The successfully synthesized KF-5 peptide demonstrated self-assembly properties, forming nanostructures in aqueous solution. At higher concentrations, these nanostructures resulted in gel-like substances with increased viscosities. Rheological studies confirmed the hydrogel-like properties of KF-5, with its storage modulus exceeding its loss modulus (Fig. S2A).

Microscopy revealed the detailed structure of the self-assembled KF-5 nanofibers. SEM revealed that KF-5 polymerizes into filamentous structures on a larger scale (Fig. 2A). TEM provided further insight, revealing a dense network of thin, well-dispersed nanofibers that formed an interconnected mesh-like structure (Fig. 2B). High-magnification TEM images allowed for a more detailed examination of the individual fibers (Fig. 2C). At higher KF-5 concentrations, the formation of hydrogel-like fibrous filaments was observed (Fig. 2D–F).

Negative staining with 3% uranyl acetate via TEM revealed intricate and well-defined nanostructures (Fig. 2G). Complementary AFM analysis provided 3D topographical information, which revealed that KF-5 formed a staggered grid-like structure (Fig. 2H–I).

FTIR spectroscopy was employed to elucidate the secondary structure of the self-assembled nanofibers (Fig. 2J). The FTIR spectrum revealed that the KF-5

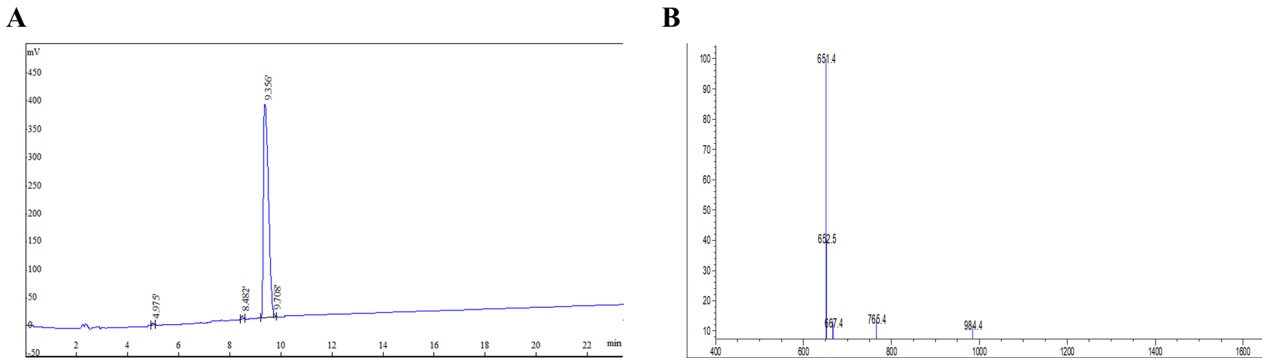

Fig. 1 Synthesis and physicochemical properties of KF-5. **A** High-performance liquid chromatography (HPLC) analysis of the KF-5 polypeptide showing a peak at a 9.35 min retention time with 98.7029% purity. **B** Mass spectrometry (MS) identification of the KF-5 polypeptide confirming the molecular weight of KF-5

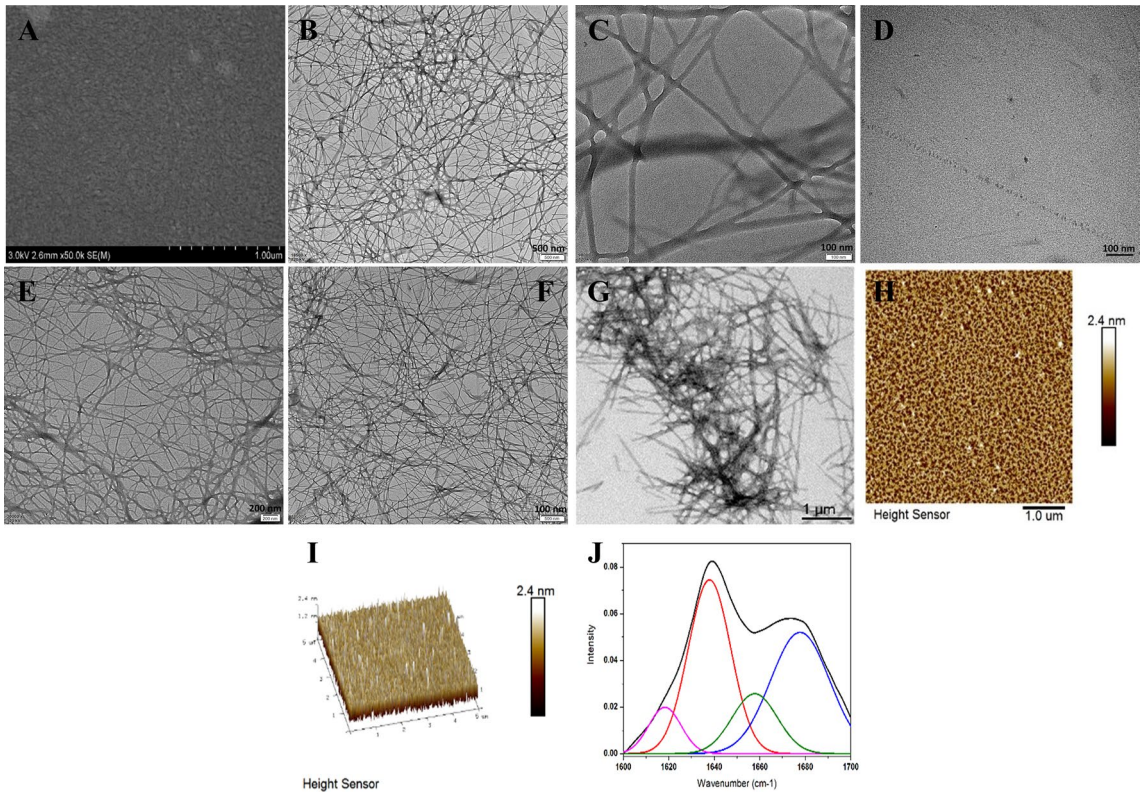

Fig. 2 Characterization of KF-5 self-assembled nanostructures. **A** Scanning electron microscopy (SEM) image showing larger-scale filamentous structures formed by the self-assembly of KF-5. **B** Low-magnification transmission electron microscopy (TEM) image showing a dense network of interconnected KF-5 nanofibers, indicating uniform self-assembly. **C** High-magnification TEM image of individual KF-5 nanofibers, revealing a fiber width of approximately 26.97 nm. (D-F) TEM images illustrating increased filament density and structural complexity at different KF-5 concentrations: **D** 1 mg/mL, **E** 2 mg/mL, and **F** 5 mg/mL. **G** TEM image of KF-5 nanostructures negatively stained with 3% uranyl acetate, highlighting the intricate arrangement of fibers. **H**, **I** Atomic force microscopy (AFM) images showing the 3D topography of KF-5 nanostructures, which form a staggered grid-like structure with a height of approximately 2.4 nm. **J** Fourier transform infrared spectroscopy (FTIR) analysis of KF-5 nanofibers, indicating that they predominantly consist of β-sheets and antiparallel β-sheets, with minimal α-helical content

Table 2 Infrared secondary structure of KF-5

Range	Structure	cm^{-1}	Ratio (%)
1610–1640	β-sheet	1618	8.00
		1637	39.60
1640–1650	Random coil	–	0.00
1650–1660	α-helix	1658	14.50
1660–1695	Antiparallel β-sheet	1677	37.90

nanofibers predominantly adopted a β-conformation. Specifically, the structure comprised approximately 50% β-sheets and antiparallel β-sheets with a small α-helical content. Notably, there was no evidence of random coiling in the nanofiber structure (Table 2).

Collectively, these findings demonstrate that the KF-5 peptide self-assembles into well-defined nanofibers with specific structural characteristics, thereby providing a foundation for understanding its potential applications and properties.

Antifungal and antibacterial activities of KF-5 against Candida albicans and Gardnerella spp.

Given that *Candida albicans* and *Gardnerella* spp. are common pathogens that cause vaginal infections, we evaluated the antibacterial efficacy of KF-5 against these organisms. The susceptibility of drug-resistant strains of *Candida albicans* and *Gardnerella* spp. obtained from clinical patients with vaginal infection with KF-5 was tested. Laser confocal microscopy revealed *Candida albicans* spores and mycelial morphology before and after KF-5 treatment (Fig. 3A and B). The antifungal effect of KF-5 against *Candida albicans* increased over time and with increasing concentration. Similar findings regarding the antibacterial effects of KF-5 were observed in *Gardnerella* spp. (Fig. 3C). After KF-5 treatment, laser confocal microscopy revealed a significant increase in the

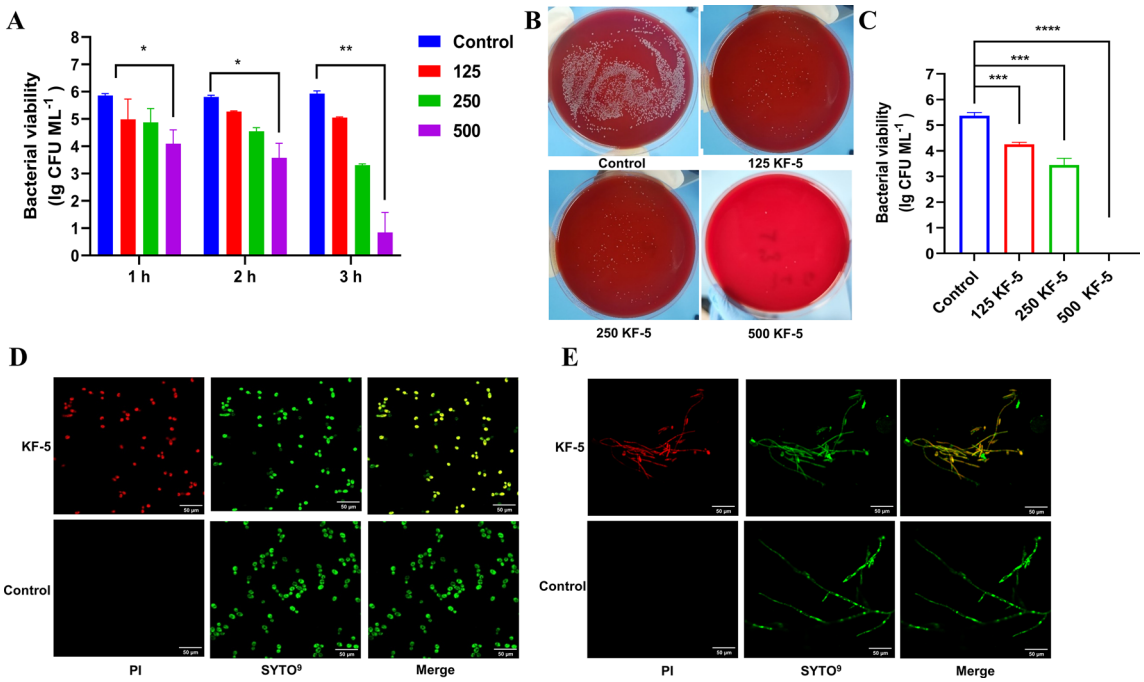

Fig. 3 Antifungal and antibacterial activities of KF-5 against *Candida albicans* and *Gardnerella vaginalis*. **A** Time-concentration gradient of KF-5 at concentrations of 0 (μg/mL) (control), 125 (μg/mL) (μg/mL), 250 and 500 (μg/mL) on *Candida albicans*. **B** Antifungal effects of 0 (μg/mL) (control), 125 (μg/mL), 250 (μg/mL) and 500 (μg/mL) KF-5 on *Candida albicans* spores. **C** Antibacterial effect of KF-5 at concentrations of 0, 125, 250 and 500 μg/ml on *Gardnerella* spp. **D**, **E** Confocal microscopy images showing the increased proportion of dead **D** *Candida albicans* spores and **E** mycelia after KF-5 treatment. Scale bar: 50 μm. The data are presented as the means ± SDs. **P* < 0.05, ***P* < 0.01, ****P* < 0.001, *****P* < 0.0001

proportion of *Gardnerella* spp. spores, *Candida albicans* spores, and mycelia that died (Fig. 3D and E & Fig. S2B).

Interaction between KF-5 and model membrane systems

Zeta potential tests revealed that the zeta potential of KF-5 was 13.2 ± 1.81 mV at pH 3, 7.25 ± 1.28 mV at pH 5, 5.42 ± 0.9 mV at pH 7, − 9.99 ± 2.21 mV at pH 9, and − 21.47 ± 1.96 mV at pH 11. The isoelectric pH (PI) of the KF-5 peptide was 7.8. KF-5 had a positive charge at pH 3, 5, and 7 but a negative charge at pH 9 and 11 (Fig. 4A). The membrane potential-sensitive probes diSC3(5) and KF-5 depolarized the membrane of *Candida albicans*, resulting in increased fluorescence (Fig. 4B). This indicated a reduction in membrane potential, as diSC3(5) was released into the solution upon membrane depolarization. Additionally, fluorescence monitoring of 8-aniline-1-naphthalene sulfonic acid (ANS) dye in *Candida albicans* cells before and after KF-5 treatment revealed a significant increase in membrane permeability (Fig. 4C). The level of lipid reactive oxygen species (ROS) in C11-BODIPY581/591, a fluorescent ratiometric probe of lipid oxidation, increased when *Candida albicans* was treated with KF-5 (Fig. 4D). Given that KF-5 has a positive charge and *Candida albicans* has a negative charge in the normally acidic environment of the human vagina, KF-5 attracts bacteria through electrostatic interactions and subsequently interacts with the bacterial cell membrane. This interaction disrupts cell membrane integrity, leading to oxidative stress and cell death. These findings provided a theoretical basis for the bactericidal effects of KF-5.

KF-5 demonstrates no toxicity to epithelial cells

The potential cytotoxicity of the KF-5 nanostructures to human cell lines was evaluated, and DMSO was used as a positive control that killed the cells in a dose-dependent manner. Using the CCK-8 assay, the viability of human vaginal epithelial cell lines (VK2), HaCaT keratinocytes, and rat macrophage RAW cell lines was assessed after treatment with KF-5 or DMSO. The results indicated that all compounds exhibited significant biocompatibility with no evident cytotoxicity. Over 95% of the cells remained viable after treatment with 1000 μg/ml KF-5 (Fig. 5A–C).

Computational antibacterial mechanism of KF-5

The antibacterial mechanism of KF-5 was investigated. The root-mean-square deviation (RMSD) values of the 10 KLVFF peptide molecules and the POPC phospholipid membrane molecules were analyzed. The results revealed that the RMSD values of 10 KLVFF peptide molecules and POPC phospholipid membrane molecules

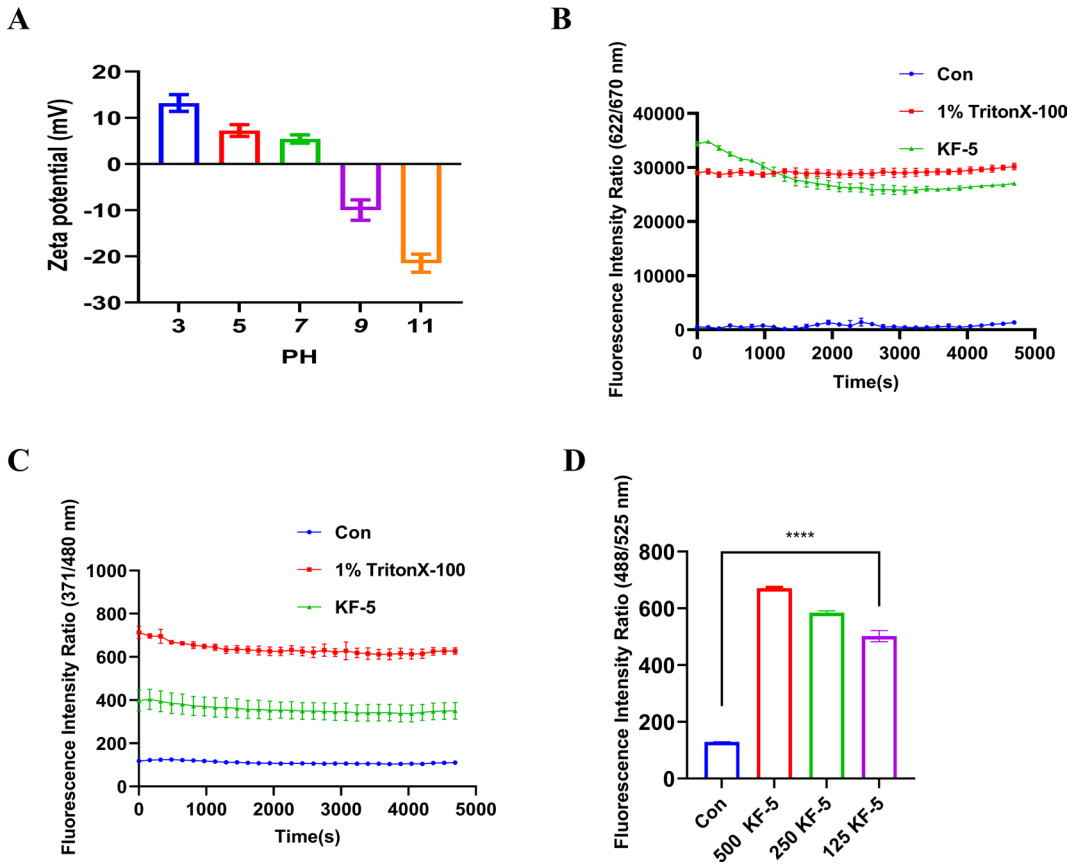

Fig. 4 KF-5 causes membrane perturbations and oxidative stress in *Candida albicans*. **A** Zeta potential of KF-5 measured at different pH values, showing positive charges at pH 3, 5, and 7 and negative charges at pH 9 and 11. **B** KF-5-induced membrane depolarization in *Candida albicans*, as measured by the increase in fluorescence of the diSC3(5) probe (Triton X-100 was used as a positive control). **C** KF-5-induced membrane permeabilization was measured via an 8-anilonapthalene-1-sulfonic acid (ANS) uptake assay (melittin was used as a positive control). **D** Lipid peroxidation in *Candida albicans* detected via C11-BODIPY581/591 after KF-5 treatment, indicating increased oxidative stress. The data are presented as the means ± SDs. ****$P < 0.0001$

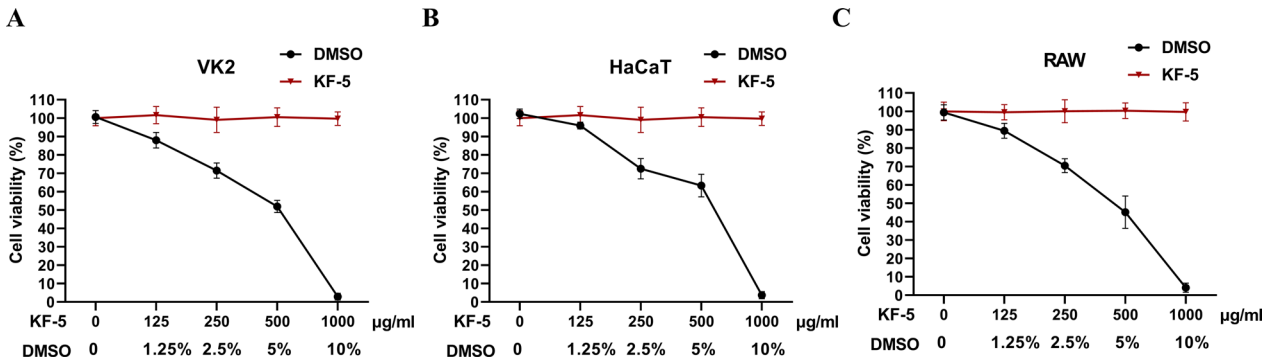

Fig. 5 Biocompatibility of KF-5 with mammalian cells. CCK-8 assays were performed to evaluate the cytotoxicity of KF-5 at concentrations of 125 (μg/mL), 250 (μg/mL), 500 (μg/mL), and 1000 (μg/mL) on **A** VK2 (human vaginal epithelial cells), **B** HaCaT (keratinocytes), and **C** RAW264.7 (rat macrophages) cells. Over 95% cell viability was maintained even after treatment with 1000 μg/mL KF-5

fluctuated during the simulation process and gradually increased compared with those of the initial structure. This finding indicates that the interaction between the peptide molecules and phospholipid membranes continued to occur during the process, and that the spatial conformations of the peptide molecules and phospholipid

membranes changed to a certain extent (Fig. 6A). The interaction energies between the KF-5 polypeptide molecules and whole phospholipid membrane molecules were subsequently calculated using the gmx_energy program and divided into van der Waals and electrostatic energies. The results showed that KLVFF polypeptide molecules bound to the surface of the POPC membrane mainly through electrostatic interactions, thereby disrupting the membrane structure (Fig. 6B). The initial structure of the phospholipid membrane was relatively uniform and the overall thickness was maintained at approximately 3.5 nm. When the peptide molecules interacted with the phospholipid molecules for 50 ns, the thickness of the entire phospholipid membrane increased significantly, the distribution became uneven, and the thickness of the localized regions increased significantly, indicating that the binding of the peptide molecules affected the structure of the phospholipid membranes and increased the thickness of the localized regions (Fig. 6C–F). Figure 6G and H show the initial and final complex structures of the system, respectively. After 50 ns of simulation, there was an obvious interaction between the peptide and the POPC phospholipid molecules. Owing to the periodicity of the box, the peptide molecules interact with the phospholipid molecules on both sides and are affected by the interaction of the peptide molecules. The structure and thickness of the POPC phospholipid membranes changed significantly. In the final complex structure, the interaction between KF-5 peptide molecules and the POPC phospholipid membrane resulted in membrane disruption, localized dilatation, and partial embedding of KF-5 molecules into the membrane surface (Fig. 6I).

KF-5 effectively moderates vaginal infection in mice

To confirm the effects of KF-5 on vaginal infection, we constructed a mouse model of vaginal infection for in vivo evaluation. We determined the antifungal effects of KF-5 on vaginal infection by colony counting, HE staining, and PAS staining. Fungal burden in the model group was significantly higher than that in the control group. Compared to the model group, the fungal burden in all three KF-5 groups was significantly reduced in a dose-dependent manner (Fig. 7A). Gram staining further revealed that many hyphae were formed during vaginal excretion in model mice, and KF-5 treatment significantly inhibited hyphal formation in a dose-dependent manner (Fig. 7B). H&E staining revealed that the vaginal mucosa of the mice in the model group was severely damaged, with obvious cellular edema and inflammatory cell infiltration. All symptoms were relieved to different degrees after KF-5 treatment. We observed that the vaginal mucosa of mice in the 1 KF-5 and 2 KF-5 groups was restored without obvious cellular edema or inflammatory cell infiltration (Fig. 7C). PAS staining revealed abundant *Candida albicans* in the vaginal tissues of the model group. In contrast, the treatment groups showed a dose-dependent reduction in *Candida albicans*, with higher concentrations of KF-5 resulting in fewer fungal cells (Fig. 7C). Next, to assess the effect of KF-5 on the inflammatory response, we performed ELISA on vaginal tissues. TNF-α and IL-6 concentrations in the model group were significantly higher than those in the control group. However, the concentrations of TNF-α and IL-6 gradually decreased with increasing KF-5 concentration (Fig. 7D). These results demonstrate that KF-5 suppresses the inflammatory response to moderate vaginal infection in mice. To further confirm the therapeutic efficacy of KF-5, we conducted in vivo and in vitro experiments to compare the effects of KF-5 and the conventional antifungal miconazole on vaginal infection. We found that the antifungal effect of KF-5 against *Candida albicans* increased with increasing concentration. Moreover, the antibacterial activity of the 500 KF-5 group was significantly greater than that of the miconazole group (Fig. S1A). In addition, H&E staining revealed that the inhibitory effect of miconazole on the infiltration of inflammatory cells in the vaginal tissues of the model mice was significantly lower than that in the 2 KF-5 group (Fig. S1B). These results suggest that KF-5 is more effective against vaginal infections compared to miconazole.

Biosafety characteristics of KF-5

To further investigate the biosafety of KF-5 in the vaginal mucosa, long-term toxicity assessment was conducted in vivo. Four groups of mice received either the blank control or different concentrations of KF-5. We found

(See figure on next page.)

Fig. 6 Simulation of the interaction between the KF-5 peptide and the 1-palmitoyl-2-oleoyl-sn-glycero-3-phosphocholine (POPC) phospholipid membrane. **A** Root-mean-square deviation (RMSD) in the molecular simulation of KF-5 and POPC phospholipid membranes. **B** The interaction energy between the KF-5 polypeptide molecule and the whole phospholipid membrane molecule, showing primarily electrostatic interactions. **C**, **D** Density distributions of the KF-5 polypeptide and POPC phospholipid in the initial and final complex structures. **E**, **F** Spatial distribution projection of the KF-5 polypeptide molecule and POPC phospholipid membrane in the initial and final complex structures. **G**, **H** KF-5 polypeptide molecule and POPC phospholipid membrane mechanism of the initial and final complex structure simulation diagrams. (I) Enlarged view of the interaction region between the KF-5 polypeptide molecule and the POPC phospholipid membrane in the final complex structure, showing local embedding of KF-5 on the membrane surface

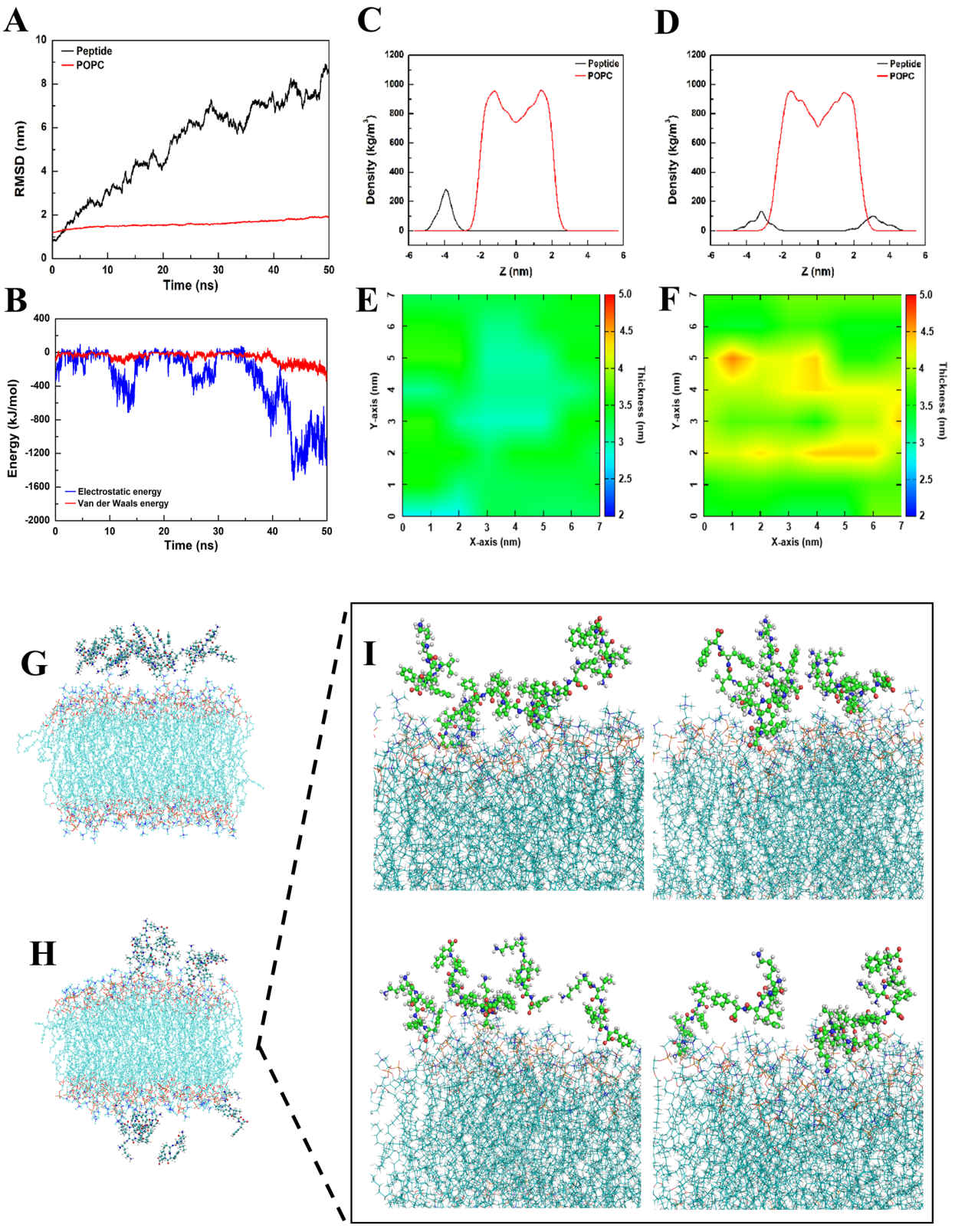

Fig. 6 (See legend on previous page.)

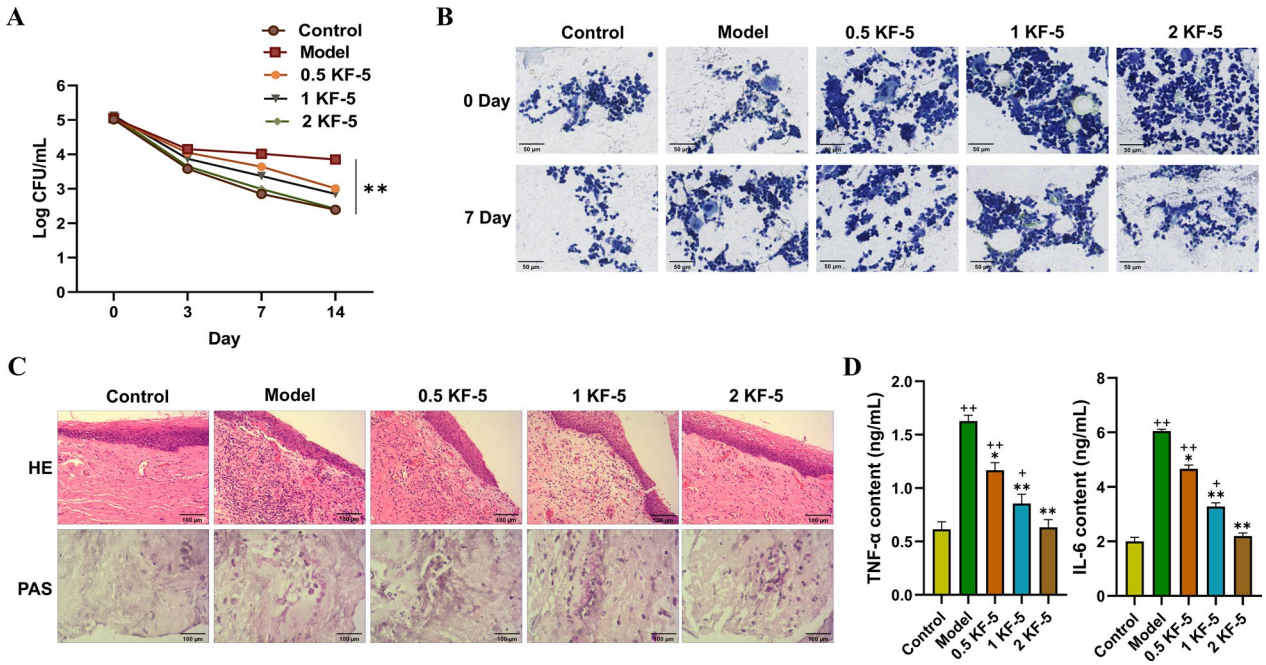

Fig. 7 KF-5 effectively moderates vaginal infection in mice. **A** Vaginal fungal burden analysis via colony counting in the vaginal lavage fluid of control, model, 0.5 (mg/mL) KF-5, 1 (mg/mL) KF-5, and 2 (mg/mL) KF-5 mice from days 1–14. Treatment was administered daily for 5 days starting on Day 0. **B** The formation of hyphae in the vaginal excreta of the mice in the control group, model group, 0.5 (mg/mL) KF-5 group, 1 (mg/mL) KF-5 group, and 2 (mg/mL) KF-5 group was determined by Gram staining on the 0th and 7th days. Scale bar: 50 μm. **C** Histopathological analysis of vaginal tissues from mice in the control group, model group, 0.5 (mg/mL) KF-5 group, 1 (mg/mL) KF-5 group, and 2 (mg/mL) KF-5 group was performed via hematoxylin and eosin (H&E) staining (top row) and periodic acid Schiff (PAS) staining (bottom row). Scale bar: 100 μm. (D) ELISA was performed to detect TNF-α and IL-6 levels in the vaginal tissues of mice in the control group, model group, 0.5 (mg/mL) KF-5 group, 1 (mg/mL) KF-5 group, and 2 (mg/mL) KF-5 group. The data are presented as the means ± SDs. + + indicates $P < 0.01$ compared with the control group. + indicates $P < 0.05$ compared with the control group. * indicates $P < 0.05$ compared with the model group. ** indicates $P < 0.01$ compared with the model

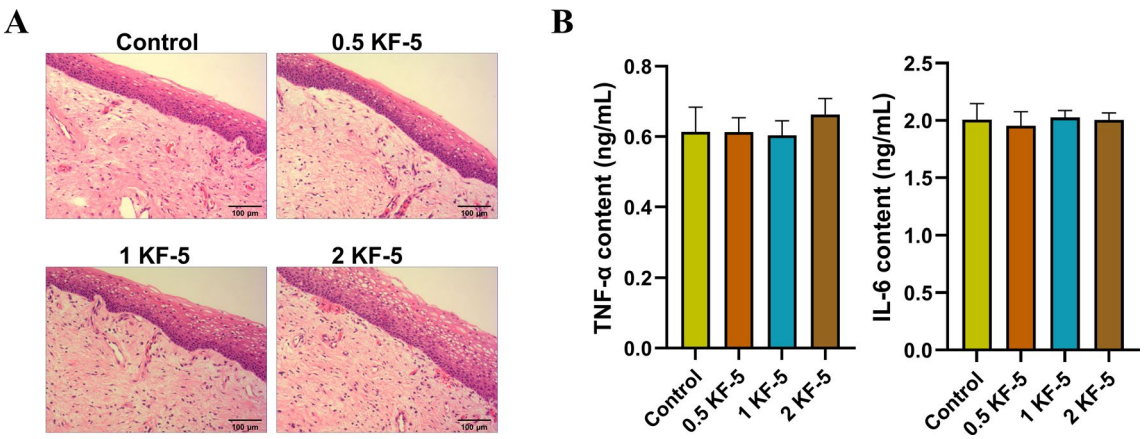

Fig. 8 Biosafety characteristics of KF-5. Toxicological evaluation of KF-5 following a repeated intravaginal daily dose for 28 days. **A** HE staining of vaginal tissues from mice in the control, 0.5 (mg/mL) KF-5, 1 (mg/mL) KF-5, and 2 (mg/mL) KF-5 groups revealed no significant epithelial damage or inflammatory cell infiltration. Scale bar: 100 μm. **B** ELISA results showing TNF-α and IL-6 levels in the vaginal tissues of different mice. No statistically significant differences were detected between the control group, 0.5 (mg/mL) KF-5 group, 1 (mg/mL) KF-5 group, and 2 (mg/mL) KF-5 group ($P > 0.05$). The data are presented as the means ± SDs

Table 3 A stability study of KF-5 polypeptide nanohydrogels

Intervals	% Inhibition			
	4 °C	Room temperature	30 °C	40 °C
Week 0	90.65 ± 1.02	91.22 ± 1.15	92.37 ± 0.53	93.72 ± 1.27
Week 1	86.28 ± 1.17	93.16 ± 1.23	94.25 ± 1.86	92.19 ± 1.59
Week 2	85.34 ± 1.47	93.89 ± 3.18	92.64 ± 2.63	91.68 ± 2.95
Week 3	90.61 ± 1.02	88.27 ± 0.59	89.67 ± 1.08	87.12 ± 1.57
Week 4	92.94 ± 0.88	95.13 ± 1.46	97.24 ± 0.85	98.36 ± 0.51
Week 5	92.17 ± 1.54	94.85 ± 0.95	92.69 ± 1.18	90.61 ± 2.61
Week 6	89.74 ± 1.67	94.67 ± 0.75	93.25 ± 0.94	88.92 ± 2.12
Week 7	92.81 ± 2.64	91.58 ± 2.35	90.67 ± 3.12	91.64 ± 1.67
Week 8	90.87 ± 1.14	92.66 ± 2.08	91.37 ± 3.84	85.74 ± 1.96

Table 4 pH and viscosity of KF-5 polypeptide nanohydrogels stored at 40 °C for 8 weeks

	0 week	8 week
pH	5.12 ± 0.036	5.23 ± 0.047
Viscosity (mPa.s)	5910 ± 19.3	5890 ± 16.5

that mice in the treatment group presented no signs of discomfort or exhibited toxic behavior. H&E staining revealed no significant epithelial damage or inflammatory cell infiltration in the vaginal tissues of the control group or any of the KF-5 treatment groups (Fig. 8A). In addition, ELISA revealed no statistically significant differences in the concentration of inflammatory factors between the control and KF-5 treatment groups (Fig. 8B). Furthermore, we tested the stability of the KF-5 polypeptide nanohydrogels at different temperatures, and the results revealed that the antibacterial effects of KF-5 stored at the specified temperature were maintained for up to eight weeks (Table 3). In addition, there was no significant change in the pH or viscosity of the KF-5 polypeptide nanohydrogels stored at 40 °C for eight weeks (Table 4). These results confirmed the stability of the KF-5 polypeptide nanohydrogels. Therefore, we believe that KF-5 could be developed as a safe and effective antibacterial agent for treating vaginal infections.

Discussion

In recent decades, amyloid β-protein (Aβ) has gained traction as the main component of β-amyloid deposits in the brains of AD patients. The understanding and investigation of Aβ has shifted from incidental catabolic byproducts to their physiological roles [43]. The pathogenicity of amyloids is associated with their pathological self-assembly. The cytotoxicity of Aβ peptides is induced by their oligomeric forms through membrane permeation, whereas the fibrillar conformations of amyloids are responsible for their interaction with the immune system to induce pro-inflammatory activities [44]. Because their biological properties are similar to those of Aβ, AMPs derived from the β-amyloid precursor protein, which can permeate microbial membranes, can inhibit the growth of microorganisms [43, 45].

However, owing to the length and complexity of amyloid proteins, it is challenging to discern the physical and chemical properties that govern their antibacterial activities. Inspired by the human amyloid protein, we derived a fragment from positions 16 to 20 of β-amyloid protein 1–42 (Aβ-1–42) using a biomimetic approach. This 5-peptide fragment is considered to be a target peptide that binds to Aβ1-42. The resulting amphiphilic polypeptide possesses the core diphenylalanine (FF) sequence required for Aβ1–42 self-assembly and can self-assemble into a β-folded amyloid fiber structure. We identified KF-5 as a fundamental self-assembly motif to further understand the implications of the interaction between self-assembly and antimicrobial activity.

Peptide drugs have novel mechanisms of action, low toxicity, high specificity, and are easy to synthesize and modify, making them promising for the treatment of infectious diseases [46]. Classical amyloid proteins and peptides, such as serum amyloid A, β-amyloid, and α-synuclein, have been confirmed to exhibit antimicrobial activities in vitro and induce innate and adaptive immunity [47, 48]. In an in vivo model, β-amyloid also exhibited protective effects against various infections [33]. Diphenylalanine nanoassemblies are of great clinical interest as core recognition motifs of β-amyloid polypeptides. To date, diphenylalanine has been reported to be the most minimalistic motif of peptide-based antimicrobial building blocks [49]. Hence, by selecting amino acids from positions 16 to 20 of the core fragment of amyloid beta 1–42 (Aβ1–42), we chemically synthesized an amphiphilic polypeptide, KF-5, or KLVFF, which was capable of self-assembling into a β-nanofiber structure in an aqueous solution. The amphiphilic polypeptide KF-5, which contains the core FF sequence required for Aβ1-42 self-assembly, forms a hydrogel-like structure. Although it shares characteristics with Aβ1-42, its shorter sequence makes it more manageable to study and less costly to design and synthesize.

Studies have shown that AMPs exhibit broad-spectrum activity against many gram-negative and gram-positive bacterial strains and fungi [50]. They have been utilized for treating candidiasis and combatting the replication of HIV1 by eliminating viral gene expression [51]. AMPs bind to the surface of anionic bacteria and can integrate into the cell membrane, forming

pores to kill microorganisms, because most AMPs are cationic and exhibit amphiphilic properties [51, 52]. In our study, KF-5 effectively killed both Gardnerella spp. and *Candida albicans* fungi and bacteria in a time- and concentration-dependent manner. Moreover, KF-5 exhibited potent fungicidal effects against fungi at different developmental stages (spores and mycelia). The proportion of dead *Candida albicans* was significantly increased after KF-5 treatment. This broad-spectrum activity is particularly valuable, given the complex nature of vaginal infections, which can involve multiple pathogens. The mechanism of action of KF-5 appears to be similar to that of other AMPs, and involves electrostatic interactions with microbial membranes. Zeta potential studies have revealed that KF-5 has a positive charge at physiological pH, which likely facilitates its interaction with negatively charged microbial membranes. The subsequent membrane depolarization and increased permeability observed in our study suggested that KF-5 disrupts membrane integrity, leading to cell death. This mechanism of action, which is distinct from that of conventional antibiotics, may contribute to the effectiveness of KF-5 against drug-resistant strains.

Interestingly, our in vivo studies revealed that KF-5 not only has antimicrobial activity, but also anti-inflammatory properties. Treatment with KF-5 significantly reduced inflammatory cell infiltration and proinflammatory cytokine levels (TNF-α and IL-6) in the vaginal tissues of the infected mice. While this effect may partially result from a reduction in pathogen load, it is possible that KF-5 directly modulates the inflammatory response. Some AMPs have been shown to interact with host immune cells and influence inflammatory signaling pathways [53, 54]. For example, Shim et al. suggested that WALK11 peptides possess both antimicrobial and anti-inflammatory activities and can inhibit TLR4 endocytosis in lipopolysaccharide-stimulated macrophages [55]. Similarly, Dong et al. revealed that OIR3 peptides can reduce skin inflammation in an allergic dermatitis mouse model by suppressing TNF-α, IL-1β, and IL-6 expression [56]. The exact mechanisms by which KF-5 exerts its anti-inflammatory effects warrant further investigation, and could expand its therapeutic applications beyond infection control.

A significant finding of our study was the superior efficacy of KF-5 compared to miconazole, a commonly used antifungal agent, in treating vaginal infections in our mouse model. Miconazole is an efficient, safe, and broad-spectrum antifungal drug that has been confirmed as the preferred topical treatment for mucosal Candida infections [57, 58]. The fact that KF-5 outperformed miconazole in our study highlights its potential as a novel therapeutic agent, particularly in the context of increased antifungal resistance.

Furthermore, our safety tests revealed that KF-5 was safe in vitro and did not cause histopathological changes in the vaginal epithelium of the mice. The excellent biocompatibility of KF-5, as demonstrated by its lack of toxicity in human vaginal epithelial cells, keratinocytes, and macrophages, is a crucial advantage for its potential as a therapeutic agent. This long-term safety study revealed no adverse effects after 28 d of daily administration, further supporting its promising safety profile.

Although our study provides compelling evidence of the therapeutic potential of KF-5, several limitations should be acknowledged. First, our findings were based on mouse models and further clinical studies are necessary to confirm their relevance in humans. Second, while we demonstrated the effectiveness of KF-5 against *Candida albicans* and *Gardnerella spp*., its impact on the broader vaginal microbiome, particularly on beneficial *Lactobacillus* species, needs to be assessed. Maintaining a healthy vaginal microbiome is crucial for long-term vaginal health, and any new treatment should be evaluated for its potential impact on this delicate microbial balance. Third, although KF-5 has potent antimicrobial effects, its potential to develop microbial resistance over time should be evaluated in future long-term studies. The molecular mechanisms underlying the anti-inflammatory effects of KF-5 should be explored in detail to identify additional therapeutic applications. Finally, the potential of KF-5 in combination therapies or in the treatment of other mucosal infections should be investigated.

Conclusion

This study demonstrated that amyloid peptides can self-assemble into nanostructures with potent bactericidal effects and excellent biocompatibility. By designing self-assembling AMPs, such as KF-5, we propose a promising alternative to traditional antibiotics, particularly for combatting bacterial resistance through diverse mechanisms of action. The self-assembled KF-5 polypeptide nanohydrogel showed potential for maintaining the balance of vaginal microbiota and could represent a novel treatment approach for vaginal infections. However, further research is needed to fully elucidate the mechanism of action, assess its long-term safety and efficacy in humans, and explore its broader therapeutic potential.

Supplementary Information

The online version contains supplementary material available at https://doi.org/10.1186/s13062-024-00546-2.

Additional file 1.

Acknowledgements
Not applicable.

Author contributions
Ling Fang: Conceptualization, Data curation, Formal analysis, Investigation, Methodology, Software, Validation, Visualization, Writing—original draft preparation. Tiancheng Yang: Conceptualization, Data curation, Formal analysis, Investigation, Methodology, Software, Validation, Visualization, Writing—original draft preparation. Haojue Wang: Conceptualization, Funding acquisition, Project administration, Resources, Supervision, Writing—review & editing. Jun Cao: Conceptualization, Funding acquisition, Project administration, Resources, Supervision, Writing—review & editing.

Funding
This study was supported by the Wuxi Municipal Health Commission Youth Project (no. Q202052), the Wuxi Science and Technology Plan Project (No. N2020X018), the Top Talent Support Program for Young and Middle-aged People of the Wuxi Health Committee (no. bj2020111, HB2023115), the Scientific Research Project Plan of the Wuxi Municipal Health Commission (No. M202007), and the National Natural Science Foundation of China (No. 82302562).

Availability of data and materials
The datasets used and analyzed in the current study are available from the corresponding author upon request. No datasets were generated or analysed during the current study.

Declarations

Ethics approval and consent to participate
All the experimental procedures were approved by the ethics committee of Nanjing Medical University.

Consent for publication
Not applicable.

Competing interests
The authors declare no competing interests.

Author details
[1]Nanjing Medical University, Nanjing 211166, Jiangsu, China. [2]Xishan People's Hospital of Wuxi City, Wuxi Branch of Zhongda Hospital Southeast University, Wuxi 214105, Jiangsu, China. [3]Jiangsu Institute of Parasitic Diseases, Wuxi 214064, Jiangsu, China.

Received: 12 June 2024 Accepted: 9 October 2024
Published online: 22 October 2024

References

1. Marnach ML, Wygant JN, Casey PM. Evaluation and management of vaginitis. Mayo Clin Proc. 2022;97(2):347–58.
2. Greenbaum S, et al. Ecological dynamics of the vaginal microbiome in relation to health and disease. Am J Obstet Gynecol. 2019;220(4):324–35.
3. Chen X, et al. The female vaginal microbiome in health and bacterial vaginosis. Front Cell Infect Microbiol. 2021;11: 631972.
4. Paczkowska M et al. Mucoadhesive Chitosan Delivery System with Chelidonii Herba Lyophilized Extract as a Promising Strategy for Vaginitis Treatment. J Clin Med 2020;9(4).
5. Peebles K, et al. High global burden and costs of bacterial vaginosis: a systematic review and meta-analysis. Sex Transm Dis. 2019;46(5):304–11.
6. Abou Chacra L, Fenollar F, Diop K. Bacterial vaginosis: what do we currently know. Front Cell Infect Microbiol. 2021;11:672429.
7. Nyirjesy P, et al. Vulvovaginal Candidiasis: a review of the evidence for the 2021 centers for disease control and prevention of sexually transmitted infections treatment guidelines. Clin Infect Dis. 2022;74(Suppl_2):S162–8.
8. Rahmoun LA, Azrad M, Peretz A. Antibiotic resistance and biofilm production capacity in clostridioides difficile. Front Cell Infect Microbiol. 2021;11: 683464.
9. Tomas M, et al. Bacterial vaginosis: standard treatments and alternative strategies. Int J Pharm. 2020;587: 119659.
10. Fatima S et al. Titanium dioxide nanoparticles induce inhibitory effects against planktonic cells and biofilms of human oral cavity isolates of *Rothia mucilaginosa*, *Georgenia* sp. and *Staphylococcus saprophyticus*. Pharmaceutics 2021; 13(10).
11. Ahmed B et al. ROS mediated destruction of cell membrane, growth and biofilms of human bacterial pathogens by stable metallic AgNPs functionalized from bell pepper extract and quercetin. Adv Powder Technol 2018; 1601–1616.
12. Khan MA, et al. Anti-quorum sensing, antibiofilm, and antibacterial activities of extracts of *Centella asiatica* L. leaves, and in vitro derived leaves-calli through tissue culture: a potential for biofouling-prevention. Biofouling. 2022;38(7):715–28.
13. Harriott MM, Noverr MC. Importance of Candida-bacterial polymicrobial biofilms in disease. Trends Microbiol. 2011;19(11):557–63.
14. Park I et al. The antibiofilm effects of antimony tin oxide nanoparticles against polymicrobial biofilms of uropathogenic *Escherichia coli* and *Staphylococcus aureus*. Pharmaceutics 2023;15(6).
15. Wang C, et al. Antimicrobial peptides towards clinical application: delivery and formulation. Adv Drug Deliv Rev. 2021;175: 113818.
16. Bin Hafeez A et al. Antimicrobial peptides: an update on classifications and databases. Int J Mol Sci 2021; **22**(21).
17. Freitas ED, et al. Antimicrobial peptides and their potential application in antiviral coating agents. Colloids Surf B Biointerf. 2022;217: 112693.
18. Gan BH, et al. The multifaceted nature of antimicrobial peptides: current synthetic chemistry approaches and future directions. Chem Soc Rev. 2021;50(13):7820–80.
19. Diez-Pascual AM, Rahdar A. Functional nanomaterials in biomedicine: current uses and potential applications. ChemMedChem. 2022;17(16): e202200142.
20. Hamley IW. PEG-peptide conjugates. Biomacromol. 2014;15(5):1543–59.
21. Abbas M et al. Self-assembled peptide- and protein-based nanomaterials for antitumor photodynamic and photothermal therapy. Adv Mater, 2017;29(12).
22. Habibi N, et al. Self-assembled peptide-based nanostructures: smart nanomaterials toward targeted drug delivery. Nano Today. 2016;11(1):41–60.
23. Moore AN, Hartgerink JD. Self-assembling multidomain peptide nanofibers for delivery of bioactive molecules and tissue regeneration. Acc Chem Res. 2017;50(4):714–22.
24. Ragonis-Bachar P, et al. Natural antimicrobial peptides self-assemble as alpha/beta chameleon amyloids. Biomacromol. 2022;23(9):3713–27.
25. Qi GB, et al. Self-assembled peptide-based nanomaterials for biomedical imaging and therapy. Adv Mater. 2018;30(22): e1703444.
26. Wei G, et al. Self-assembling peptide and protein amyloids: from structure to tailored function in nanotechnology. Chem Soc Rev. 2017;46(15):4661–708.
27. Chu H, et al. Human alpha-defensin 6 promotes mucosal innate immunity through self-assembled peptide nanonets. Science. 2012;337(6093):477–81.
28. Chen W, et al. Self-assembled peptide nanofibers display natural antimicrobial peptides to selectively kill bacteria without compromising cytocompatibility. ACS Appl Mater Interf. 2019;11(32):28681–9.
29. Xie YY, et al. Self-assembly of peptide nanofibers with chirality-encoded antimicrobial activity. J Colloid Interface Sci. 2022;622:135–46.
30. Kagan BL, et al. Antimicrobial properties of amyloid peptides. Mol Pharm. 2012;9(4):708–17.
31. Chen D, et al. Amyloid peptides with antimicrobial and/or microbial agglutination activity. Appl Microbiol Biotechnol. 2022;106(23):7711–20.

32. Wang L, et al. Antimicrobial activity of human islet amyloid polypeptides: an insight into amyloid peptides' connection with antimicrobial peptides. Biol Chem. 2012;393(7):641–6.
33. Kumar DK, et al. Amyloid-beta peptide protects against microbial infection in mouse and worm models of alzheimer's disease. Sci Transl Med. 2016;8(340):340ra72.
34. Zhang H, et al. Interaction between Aβ and Tau in the pathogenesis of alzheimer's disease. Int J Biol Sci. 2021;17(9):2181–92.
35. Yu H, Wu J. Amyloid-beta: a double agent in Alzheimer's disease? Biomed Pharmacother. 2021;139: 111575.
36. Bourgade K, et al. beta-amyloid peptides display protective activity against the human alzheimer's disease-associated herpes simplex virus-1. Biogerontology. 2015;16(1):85–98.
37. Eimer WA, et al. Alzheimer's disease-associated beta-amyloid is rapidly seeded by herpesviridae to protect against brain infection. Neuron. 2018;100(6):1527–32.
38. Cheng R, et al. Characterization of the transcriptional response of Candida parapsilosis to the antifungal peptide MAF-1A. PeerJ. 2020;8: e9767.
39. Hess B, et al. GROMACS 4: algorithms for highly efficient, load-balanced, and scalable molecular simulation. J Chem Theory Comput. 2008;4(3):435–47.
40. Rappe AK, et al. UFF, a full periodic table force field for molecular mechanics and molecular dynamics simulations. J Am Chem Soc. 1992;114(25):10024–35.
41. Essmann U, et al. A smooth particle mesh Ewald method. J Chem Phys. 1995;103(19):8577–93.
42. Hess B, et al. LINCS: a linear constraint solver for molecular simulations. J Comput Chem. 1997;18(12):1463–72.
43. Soscia SJ, et al. The Alzheimer's disease-associated amyloid beta-protein is an antimicrobial peptide. PLoS ONE. 2010;5(3): e9505.
44. Lee EY, et al. Functional reciprocity of amyloids and antimicrobial peptides: rethinking the role of supramolecular assembly in host defense, immune activation, and inflammation. Front Immunol. 2020;11:1629.
45. Papareddy P, et al. Antimicrobial activity of peptides derived from human ss-amyloid precursor protein. J Pept Sci. 2012;18(3):183–91.
46. Lombardi L et al. A new hope: self-assembling peptides with antimicrobial activity. Pharmaceutics 2019; 11(4).
47. White MR, et al. Alzheimer's associated beta-amyloid protein inhibits influenza A virus and modulates viral interactions with phagocytes. PLoS ONE. 2014;9(7): e101364.
48. Salminen A, et al. Inflammation in Alzheimer's disease: amyloid-beta oligomers trigger innate immunity defence via pattern recognition receptors. Prog Neurobiol. 2009;87(3):181–94.
49. Schnaider L, et al. Self-assembling dipeptide antibacterial nanostructures with membrane disrupting activity. Nat Commun. 2017;8(1):1365.
50. Chung PY, Khanum R. Antimicrobial peptides as potential anti-biofilm agents against multidrug-resistant bacteria. J Microbiol Immunol Infect. 2017;50(4):405–10.
51. Wachinger M, et al. Antimicrobial peptides melittin and cecropin inhibit replication of human immunodeficiency virus 1 by suppressing viral gene expression. J Gen Virol. 1998;79(Pt 4):731–40.
52. Brown KL, Hancock RE. Cationic host defense (antimicrobial) peptides. Curr Opin Immunol. 2006;18(1):24–30.
53. Luo Y, Song Y. Mechanism of antimicrobial peptides: antimicrobial, anti-inflammatory and antibiofilm activities. Int J Mol Sci 2021; 22(21).
54. Chen X, et al. Antimicrobial peptides human beta-defensin (hBD)-3 and hBD-4 activate mast cells and increase skin vascular permeability. Eur J Immunol. 2007;37(2):434–44.
55. Shim DW, et al. Anti-inflammatory action of an antimicrobial model peptide that suppresses the TRIF-dependent signaling pathway via inhibition of toll-like receptor 4 endocytosis in lipopolysaccharide-stimulated macrophages. PLoS ONE. 2015;10(5): e0126871.
56. Dong N et al. Simplified head-to-tail cyclic polypeptides as biomaterial-associated antimicrobials with endotoxin neutralizing and anti-inflammatory capabilities. Int J Mol Sci 2019; 20(23).
57. Regidor PA, et al. Miconazole for the treatment of vulvovaginal candidiasis. In vitro, in vivo and clinical results Review of the literature. J Obstet Gynaecol. 2023;43(1):2195001.
58. Fischer TJ, et al. Miconazole in the treatment of chronic mucocutaneous candidiasis: a preliminary report. J Pediatr. 1977;91(5):815–9.

Publisher's Note